Pergamon

PII: S0038–092X(00)00149–3

Solar Energy Vol. 70, No. 4, pp. 349–359, 2001

0038-092X/01/$ - see front matter

www.elsevier.com/locate/solener

A THERMAL MODEL FOR PHOTOVOLTAIC SYSTEMS

A. D. JONES and C. P. UNDERWOOD†
School of the Built Environment, University of Northumbria, Newcastle upon Tyne NE1 ST, UK

Received 4 December 1999; revised version accepted 4 September 2000

Communicated by HANSJÖRG GABLER

Abstract—The energy balance of photovoltaic (PV) cells is modelled based on climate variables. Module temperature change is shown to be in a non-steady state with respect to time. Theoretical expressions model the energy transfer processes involved: short wave radiation, long wave radiation, convection and electrical energy production. The combined model is found to agree well with the response of the measured model temperature to transient changes in irradiance. It is found that the most precise fit to measured data is obtained by fitting the value of the forced convection coefficient for module convection. The fitted values of this coefficient were found to be within the range predicted by previous authors. Though the model is found to be accurate to within 6 K of measured temperature values 95% of the time in cloudy conditions, best accuracy is obtained in clear and overcast conditions when irradiance is subject to less fluctuation. © 2001 Elsevier Science Ltd. All rights reserved.

1. INTRODUCTION

The PV module cell temperature is a function of the physical variables of the PV cell material, the module and its configuration, the prevailing weather conditions and the surrounding environment.

Various authors have modelled the temperature of a PV module by evaluation of energy inputs and outputs through radiation, convection, conduction and power generated. Anis *et al.* (1983) lump the contributions together in an overall heat loss coefficient, resulting in a linear relationship between module temperature and irradiance under steady state conditions. Fuentes (1984) evaluates a nominal operating cell temperature for a variety of configurations. Schott (1985) also expresses the thermal energy balance as a linear equation restricted to steady state conditions. Knaup's (1992) description evaluates module heat capacity from experimental measurements and models heat transfer for non-steady state conditions.

Previously, Wilshaw *et al.* (1996) conducted a linear regression fit relating the difference of module and ambient temperature to irradiance at ambient temperatures (in effect, the overall heat transfer coefficient) between 21 and 27°C. This was based on data from the Northumberland Building PV array; a large demonstration array mounted on the south face of the Northumberland Building at the University of Northumbria, Newcastle upon Tyne, UK. The result was evaluated to be 0.035 K/(W m^{-2}) for measurements from a warm week in August.

Simple thermal models assume the period of measurement of mean power output is much greater than the period of thermal response of the module. A mean temperature is calculated essentially in a steady state condition. In the case of the 1-min data of the Northumberland Building, it shall be shown that the thermal response time of the module is significant compared to the period of measurement. Thus it is necessary to consider the thermal mass of the module in the heat transfer model. From theoretical considerations, an expression for module temperature in terms of irradiance and ambient temperature will be derived. The non-steady state model derived here is based upon the theoretical description of module temperature described by Schott (1985). The details of individual contributions are adapted from this previous work to the Northumberland Building array characteristics. The validity of the relationship will be verified with actual data from the Northumberland Building.

2. OBSERVED TEMPERATURE CHARACTERISTICS OF MODULE

A steady state model of module temperature cannot be justified during periods of rapidly fluctuating irradiance where the response time

†Author to whom correspondence should be addressed. Tel.: +44-191-227-3533; fax: +44-191-227-3167; e-mail: chris.underwood@unn.ac.uk

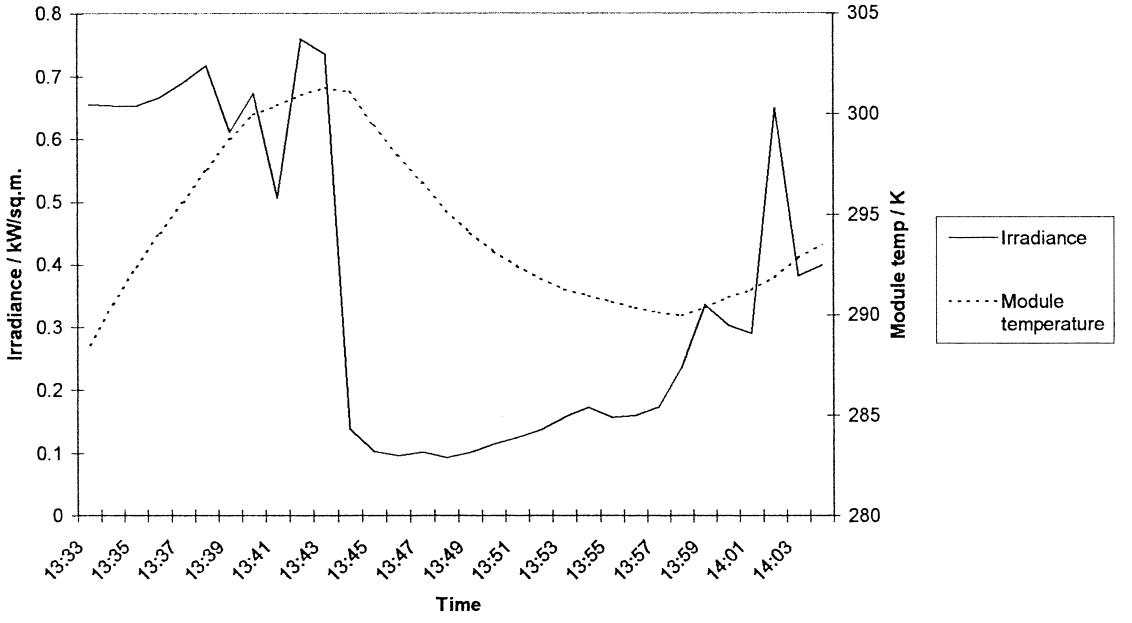

Fig. 1. Module temperature response to rapid step change in irradiance (data from 3/2/96).

caused by the thermal mass of the PV material becomes significant. Fig. 1 illustrates the module temperature response to the case of a very rapid drop in the irradiance level over a short period of time — a decrease of 0.6 kW/m^2 in 1 min, approximately a step change in irradiance. The module temperature clearly follows an exponential decay, lagging behind the step. During periods of rapidly moving cloud, the peaks and troughs of the module temperature values are seen to lag behind those of the irradiance values. Clearly, using a 1-min time period of measurement, the thermal response of the module is significant.

The time constant of the module response is defined as the time taken for the module temperature to reach 63% of the total change in temperature resulting from a step change in the irradiance level. In the case shown in Fig. 1, the total drop in temperature is ~11 K, 63% of 11 K is roughly 7 K. From the curve shown the time constant of the module is observed to be ~7 min under these conditions. It is noted that a 1-min measurement interval may not be sufficient to observe every subtlety of the thermal behaviour of the PV module.

3. MODULE TEMPERATURE MODEL

The module temperature is estimated by considering the thermal energy exchange of the module with its environment through the main heat transfer paths. In non-steady state conditions, the rate of change of module temperature with time is considered to be significantly greater than zero. The three modes of heat transfer are conduction, convection and radiation. Energy is also taken from the module in the form of the electrical energy generated. Fig. 2 shows the main heat transfer paths to and from the module.

Convection and radiation heat transfer from the front and back surfaces of the module are considered significant, whilst heat conducted from the array to the structural framework and the building is considered negligible due to the small area of contact points. The resulting rate of temperature change with time may be expressed as the sum of these contributions:

$$C_{\text{module}} \frac{\mathrm{d}T}{\mathrm{d}t} = q_{\text{lw}} + q_{\text{sw}} + q_{\text{conv}} - P_{\text{out}}. \qquad (1)$$

To solve Eq. (1) it is necessary to explicitly state the forms of each of the long and short wave

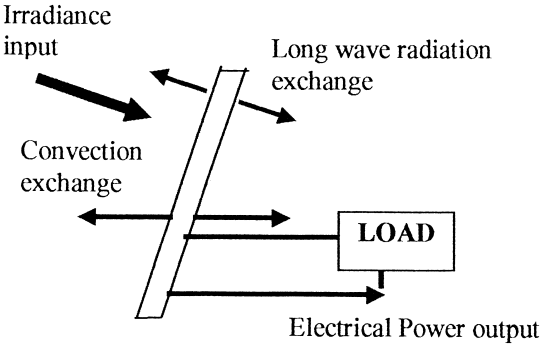

Fig. 2. Heat transfer energy exchange at PV module.

radiative exchange, the convective exchange and the power generated in terms of the characteristics of the solar module and the environmental variables.

3.1. Module heat capacity

For the purposes of calculating the effective heat capacity of the module for prediction of PV surface temperature, the module is considered as three layers of material: a flat sheet of PV cells laminated within a Polyester/Tedlar trilaminate, behind a glass face (BP Solar). The module temperature is assumed uniform throughout the three layers. The sealing materials and the frame, comprising a low surface area of the module, have a negligible effect on the temperature of the PV material and are neglected in the calculation. The module heat capacity is the sum of the heat capacities of the individual elements of the module:

$$C_{\text{module}} = \sum_{m} A \cdot d_{\text{m}} \cdot \rho_{\text{m}} \cdot C_{\text{m}} \tag{2}$$

for each component made of some material, signified by *m*.

Table 1 summarises the dimension and heat capacity and density of each of the PV module elements. The area of PV material in the module is 0.51 m^2, and a similar area of glass and polyester trilaminate is considered relevant in calculating the module heat capacity.

3.2. Short wave radiation heat transfer

The effective radiation reaching the front surface of the cell is a function of the intensity of the direct and diffuse short wave radiation inputs, and the absorptivity of the cell face. Incident short wave radiation intensity values are recorded via a pyranometer on the Northumberland Building, in the plane of the solar modules. The pyranometer does not distinguish between direct and diffuse radiation, and has a measurement band width of wavelengths 305 to 2800 nm (Kipp and Zonen). The net short wave input on the module front surface can be expressed as:

$$q_{\text{sw}} = \alpha \cdot \Phi \cdot A. \tag{3}$$

The absorptivity is a function of the orientation and configuration of the array, absorptive and reflective properties of the laminating material, encapsulating glass and the absorptivity characteristics of the PV cell material. For silicon, ~77% of solar irradiance photons are of the proper energy range to be absorbed by the PV (Merrigan, 1982). The BP585 solar module has an anti-reflection coating which decreases reflection losses to 10% (BP Solar); 10% reflectivity losses of the remaining photons give an absorptivity of 0.7. A constant absorptivity is a simplification for the calculation of values during the central daytime period. In practice, the absorptivity value is dependent on sun position, with a 20–30% reduction at small values of incident radiation (i.e. at dawn and dusk) (Schott, 1985).

3.3. Long wave radiation heat transfer

The rate of long wave electromagnetic energy radiation per unit area of a body at surface temperature T is given by the Stefan–Boltzmann law:

$$q_{\text{lw}} = \sigma \cdot \varepsilon \cdot T^4. \tag{4}$$

The fraction of radiation leaving one surface that reaches the other is known as the view factor (Holman, 1992). The net long wave radiation exchange between surfaces x and y is given by:

$$\begin{aligned} q_{\text{lw}_{xy}} &= A_x \cdot F_{xy} \cdot (L_x - L_y) \\ &= A_y \cdot F_{yx} \cdot (L_y - L_x). \end{aligned} \tag{5}$$

The rear of the module is assumed, for simplicity, to be close to the same temperature as the building fabric that it faces, and the net long wave exchange between the two surfaces is thus negligible. Thus it is only necessary to calculate the long wave exchange from the front surface of the module. If not overlooked by adjacent buildings, a tilted surface at angle β_{surface} from the horizontal has a view factor of $(1+\cos(\beta_{\text{surface}}))/2$ for the

Table 1. BP 585 module heat capacity data (sources of data BP Solar, James and Lord (1992), NPAC (1997))

Element of module	ρ_{m} (kg/m^3)	C_{m} (J/kg K)	d_{m} (m)	$A \times d_{\text{m}} \times \rho_{\text{m}} \times C_{\text{m}}$ (J/K)
Monocrystalline silicon PV cells	2330	677	0.0003	241
Polyester/Tedlar trilaminate	1200	1250	0.0005	382
Glass face	3000	500	0.003	2295
Total				2918

sky and $(1-\cos(\beta_{surface}))/2$ for the horizontal ground (Liu and Jordan, 1963).

Inserting coefficients for sky, ground and module and combining the previous two equations, the net energy exchange at the module surface is:

$$q_{lw} = A \cdot \sigma\left(\frac{(1+\cos\beta_{surface})}{2}\varepsilon_{sky} \cdot T_{sky}^4 + \frac{(1-\cos\beta_{surface})}{2}\varepsilon_{ground} \cdot T_{ground}^4 - \varepsilon_{module} \cdot T_{module}^4\right). \quad (6)$$

Values for the parameters are from Schott (1985): $\varepsilon_{sky}=0.95$ for clear conditions; 1.0 for overcast conditions, $\varepsilon_{ground}=0.95$, $\varepsilon_{module}=0.9$, $T_{sky}=(T_{ambient}-\delta T)$ for clear sky conditions in which $\delta T = 20$ K, $T_{sky}=T_{ambient}$ for overcast conditions.

3.4. Convection heat transfer

Newton's law of cooling expresses the convective energy exchange from a surface to the surrounding fluid as being proportional to the overall temperature difference between the surface and the fluid. For a PV module in air, the total convective energy exchange from a module surface is:

$$q_{conv} = -h_c \cdot A \cdot (T_{module} - T_{ambient}). \quad (7)$$

The value of the convective heat transfer coefficient h_c depends on the physical situation. Convection may be a combination of free and forced convection effects. On calm days, and on the sheltered rear side of the array, free convection will be the major form of cooling. When the exposed front of the array experiences wind, which is in most cases, forced convection will predominate.

For free cooling, if predominantly turbulent flow is assumed, the convective coefficient is proportional to some power of the temperature difference between the array and the air. An approximation given by Holman (1992) for free convection from a vertical plane in air is used to calculate the free convection coefficient of the PV module:

$$h_{c,free} = 1.31 \cdot (T_{module} - T_{ambient})^{1/3}. \quad (8)$$

The constant of proportionality (1.31) in the empirical expression of Eq. (8) has the units $W/(m^2\ K^{3/2})$.

The free convection plane in the present work lies on the rear side of the PV module where the modules are enclosed from wind effects and the plane is at an acute angle to the horizontal. In this situation, buoyancy-driven free convection was assumed to dominate events, hence the empirical expression of Eq. (8) was chosen in which the surface-to-air temperature difference is allowed to dominate the surface convection coefficient result.

On typical days, the overall convection heat transfer is the sum of the forced convection from the front surface and the free convection from the rear surface:

$$q_{conv} = -(h_{c,forced} + h_{c,free}) \cdot A \cdot (T_{module} - T_{ambient}). \quad (9)$$

For forced cooling, some authors suggest the convection coefficient $h_{c,forced}$ can be approximated as a linear function of wind speed (Schott, 1985). However, wind speeds experienced by the Northumberland Array are not recorded by the rooftop weather monitoring station, thus the impact of wind speed on T_{module} cannot be evaluated. A study of the literature reveals a considerable range of values for the forced convection coefficient. For a wind speed of 1 m/s, the value of h_c is 1.2 W/m^2 K (ASHRAE, 1989), 5.8 W/m^2 K (Anis *et al.*, 1983), 9.1 W/m^2 K (Schott, 1985) or 9.6 W/m^2 K (Pratt, 1981).

The variations of theoretical models provided in the literature, and the lack of Northumberland array wind speed data, justify finding an empirical value of the forced convection coefficient for the Northumberland building array. This will involve finding the best coefficient value for the prevailing wind conditions, which will be verified as within the range of values suggested in the literature.

3.5. Electrical power generation

The DC power output of the array is monitored at 1-min intervals. For simplicity, uniform output is assumed from all 465 PV modules in the array. The power output is modelled by a fill factor model, which may be concisely written as:

$$P_{out} = C_{FF} \cdot \frac{E \ln(k_1 E)}{T_{module}}. \quad (10)$$

3.6. Theoretical model of module temperature

Substituting Eqs. (2), (3), (6), (9) and (10) into Eq. (1) gives the following expression for rate of temperature change of a module in the Northumberland Building array

$$C_{\text{module}}\frac{\mathrm{d}T_{\text{module}}}{\mathrm{d}t} = \sigma \cdot A \cdot (\varepsilon_{\text{sky}}(T_{\text{ambient}} - \delta T)^4 - \varepsilon_{\text{module}} T^4_{\text{module}}) + \alpha \cdot \Phi \cdot A - \frac{C_{\text{FF}} \cdot E \cdot \ln(k_1 E)}{T_{\text{module}}} - (h_{\text{c,forced}} + h_{\text{c,free}}) \cdot A \cdot (T_{\text{module}} - T_{\text{amb}}) \quad (11)$$

(in which δT is 20 K for clear sky conditions).

4. EXPERIMENTAL VERIFICATION

4.1. Data selection

The data required are time series of 1-min measurements of module temperature, ambient temperature, array output and incident irradiance in the plane of the array. All measurements are taken from the monitoring of the PV clad façade of the Northumberland Building on the city centre campus of the University of Northumbria (Hill and Pearsall, 1994). It is a five-storey building with its long facades oriented approximately east–west, with the PV array on the south face of the building. The array comprises five strips of cladding along the south face of the building, the temperature measurements are made by a thermocouple embedded in a monocrystalline type BP585 PV module on the exterior of the fourth floor of the building. The modules are sealed within aluminium rainscreen overcladding units. The array is made up of cladding units which each consist of five modules. Each unit is inclined at 25° to the vertical. Electrical interconnection is carried out via wall-mounted junction boxes behind the cladding units. The total DC output of the connected cells is converted to AC electricity via an inverter unit. A maximum power point tracker in the inverter unit sets the power output at the voltage to maintain maximum power. The AC output is then connected to the main building bus in the basement electrical room.

The power output of each individual string of 15 modules is continuously monitored by a Solartron Isolated Measurement Pod system. This system also monitors the total array output DC power and inverter output AC power. Embedded type II thermocouples in five modules measure module temperature. A roof mounted weather monitoring station includes Kipp and Zonen CM11 pyranometers measuring incident irradiance on the horizontal plane and on the plane of the array. A shielded thermistor measures ambient temperature. All PV array and weather measurements are logged at 1-min intervals and retained by the Northumbria Photovoltaic Applications Centre (NPAC). The measurement uncertainties of the monitored values are:

Ambient temperature:	±0.5 K
Module temperature:	±0.5 K
Irradiance:	±0.01 kW/m^2
Array DC output power:	±0.01 kW
Inverter AC input power:	±0.01 kW

4.2. Selection of calculation method

The differential equation of module temperature change (Eq. (11)) is non-linear with no analytical solution. It must therefore be solved numerically for each set of irradiance and temperature values. The Euler method of integration of a differential equation was found to be as suitable for these calculations as more detailed alternatives (e.g. the Runge–Kutta method).

The Euler method calculation of T_{module} at time step $(t+1)$, given T_{module} at time step (t) and the rate of change from Eq. (11), is by:

$$T_{\text{module}}(t+1) = T_{\text{module}}(t) + step \cdot \frac{\mathrm{d}T_{\text{module}}}{\mathrm{d}t}. \quad (12)$$

The Euler method is an initial value method; for the first time step, a value of T_{module} is required. For testing of the model against actual data, a measured starting value of T_{module} will be used (see also Section 4.9).

4.3. Calculation of forced convection coefficient

It was noted previously that considerable differences existed in the literature on the calculation of $h_{\text{c,forced}}$, the forced convection heat transfer coefficient for a building surface. In this section, existing wind speed data from a nearby weather station shall be used to estimate $h_{\text{c,forced}}$.

Wind speed measurements are logged by the Newcastle Meteorological Office. The Newcastle weather station is close (1/4 mile) to the Northumberland Building. This station is on a roof, more exposed than the Northumberland Building array. It would be reasonable to assume that mean wind speeds in the vicinity of the array on the south face of the Northumberland Building are proportional, but lower, to those measured on the roof of the Newcastle Meteorological Office.

To observe the effect changing wind conditions have on the temperature of the modules, two

Table 2. Average hourly wind speeds as measured by Newcastle Met Office

Date	Wind speed (m/s)	
	14:00–15:00	15:00–16:00
15 August 1996	2.5	3.1
17 August 1996	6.7	6.2

periods of similar climate but different mean wind speeds are compared. The 15th and 17th August afternoons between 14:00 and 16:00 h were identified as having near identical conditions for all environmental variables except wind speed. The average wind speeds in m/s for these 2 h are shown in Table 2. With all other weather conditions constant for practical purposes on the 2 days, wind speed on the 17th is double that of the 15th. By comparison with other data, the wind speeds on the 15th are observed to be approximately average for Newcastle upon Tyne, whereas those on the 17th are above average.

It is clear from the separation of the solid measured module temperature curves shown in Fig. 3 that the increased wind speed does have an increased cooling effect on the modules on the 17th. The decrease in temperature due to the additional wind varies between 2 and 5 K. Fitting values of the forced convection coefficient $h_{c,forced}$ to large sets of data was used to establish a simple rule of thumb, that best fit the temperature data with all other coefficients remaining constant. Approximate 'best fit' values of $h_{c,forced}$ were found to be $h_{c,forced}=2$ W/m^2 K for average wind conditions (e.g. 15 August) and $h_{c,forced}=4$ W/m^2 K for above average conditions (e.g. 17 August). The best fit curves of T_{module} are shown in Fig. 3. In the case of this model, the forced convection coefficient is found to be similar in value to the calculated free convection coefficient, particularly in the case of large temperature difference between the module and surrounding air.

In conclusion, the empirical values of $h_{c,forced}$ are within the range of those quoted in the literature. It would be desirable to verify these values in more detailed experimental conditions with controlled conditions and measurements of airflow over the surface of the PV module. However, the current approximation appears appropriate for the model of module temperature postulated as the fitted value is verified against the range of values of the work of previous authors, where the range of values is from 1.9 to 9. In the following applications of the heat transfer model, $h_{c,forced}$ is set according to the wind conditions during the period of measurement. Unless otherwise specified, the prevailing wind conditions for the example periods are average for this location (i.e. ~2–3 m s^{-1}) for which $h_{c,forced}=2$ W/m^2 K.

4.4. Verification of model with measured data under various conditions

The model is used to simulate module temperature using sets of climate data selected from August and November 1995 and May 1996, so

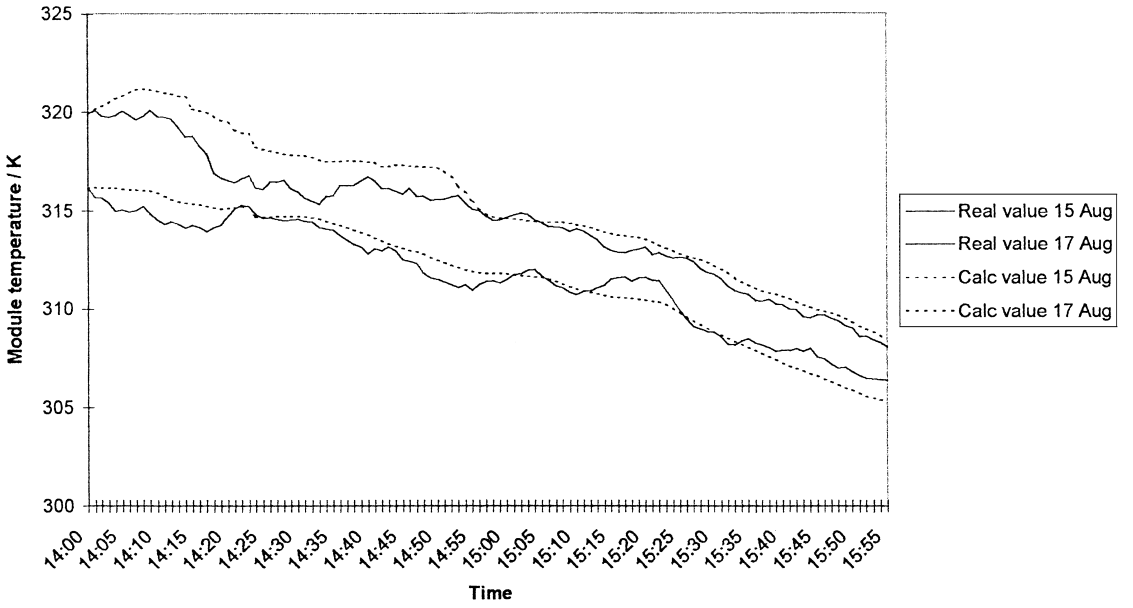

Fig. 3. Actual and calculated module temperatures on days of different wind conditions (data from 15/8/96 ($h_c=2$) and 17/8/96 ($h_c=4$)).

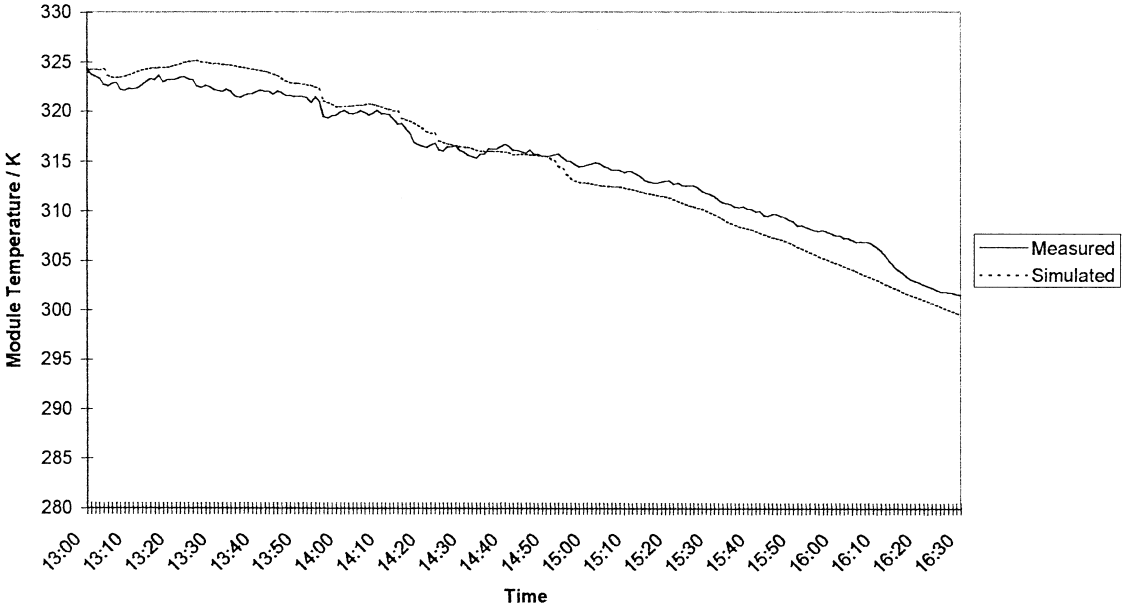

Fig. 4. Measured and simulated module temperature during period of clear sky conditions (data from 15/8/96).

that a range of ambient temperature conditions are obtained. Three main types of irradiance conditions are identified: clear sky, cloudy sky and overcast sky conditions. Evaluations of the model are presented separately for each condition. The hours selected for the verification are those when the array is negligibly shaded. The module temperature at the initial time step is set at the actual initial measured temperature.

4.5. Clear sky conditions

Fig. 4 shows the measured and simulated module temperature for a period of clear conditions. Under clear conditions the change in module temperature is very gradual, in this case, with the diminishing irradiance during the afternoon. The simulated temperature closely follows the measured temperature curve, with a difference of generally less than 3 K.

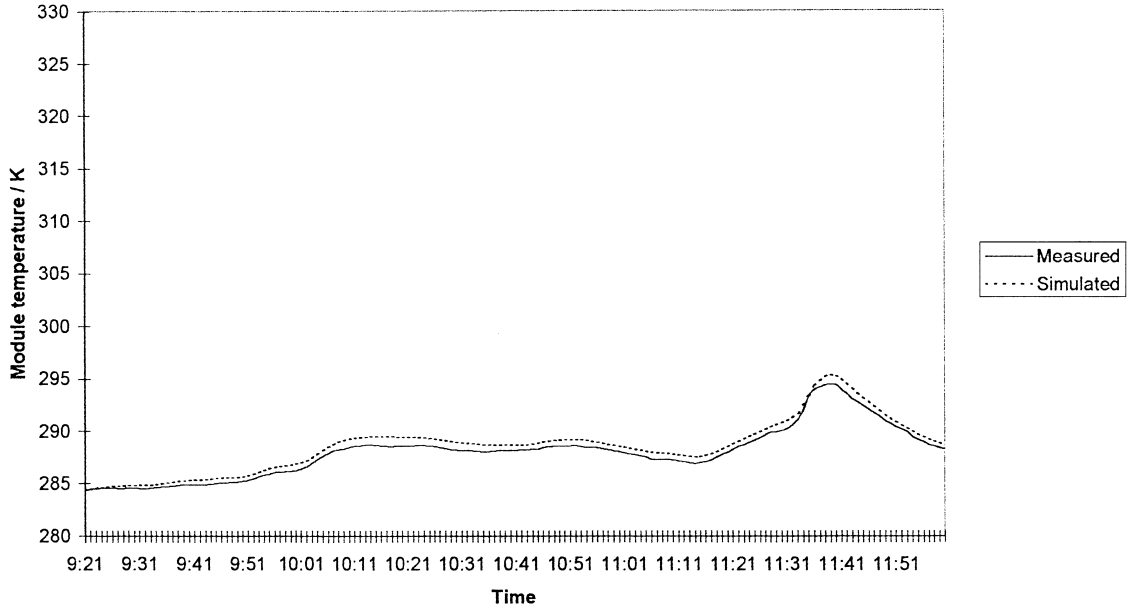

Fig. 5. Measured and simulated module temperature during period of overcast sky conditions (data from 1/11/96).

4.6. Overcast sky conditions

Fig. 5 shows the measured and simulated module temperature for a period of overcast conditions in November 1995 (above average wind $h_{c,forced} = 4$ W/m^2 K). As with clear conditions, the simulated temperature closely follows the measured temperature. The difference between the measured and calculated temperature is lower than for clear sky conditions, however, the range of temperatures measured for overcast conditions is also lower.

4.7. Cloudy sky conditions

Fig. 6 shows the measured and simulated module temperature for a period of cloudy conditions. The irradiance value varies strongly during this period, and there is a resulting variation in module temperature. The modelled temperature follows the trend of the measured temperature well. The thermal lag of the module temperature is tracked by the model, although there is a slight underestimation in some periods.

4.8. Summary of verification of temperature model

The calculated standard errors of the model used for each irradiance condition are given in Table 3. As previously observed, the accuracy of the model is best for overcast conditions and worst for cloudy conditions; 95% of modelled values will fall within two times the standard error of the measured value.

Table 3. Standard errors of estimates made by temperature model during unshaded periods

Irradiance conditions	Standard error of predicted T_{module} (K)
Clear	2.3
Cloudy	3.0
Overcast	1.2

Under clear conditions, the model performs fairly well in estimating module temperature. The module temperature tends to vary less under overcast conditions, and the precision of estimated values improves. The difference between modelled and measured temperatures is greatest under the conditions of cloudy weather compared to clear and overcast due to the existence of the rapid irradiance changes influencing the module temperature. Although the model accounts for the irradiance changes and the thermal response of the module very well, there is a natural increase in the error of estimation in these conditions.

The contributions of the individual modes of energy transfer to the overall rate of change of temperature in this model are considered. It is found that, for irradiance greater than 0.1 kW/m^2, the main cause of module temperature change is the temperature increase by absorption of short wave radiation. The negative contribution to the rate of temperature change through convective cooling is observed to have approximately half the magnitude of the short wave contribution. The electrical and long wave emission contributions

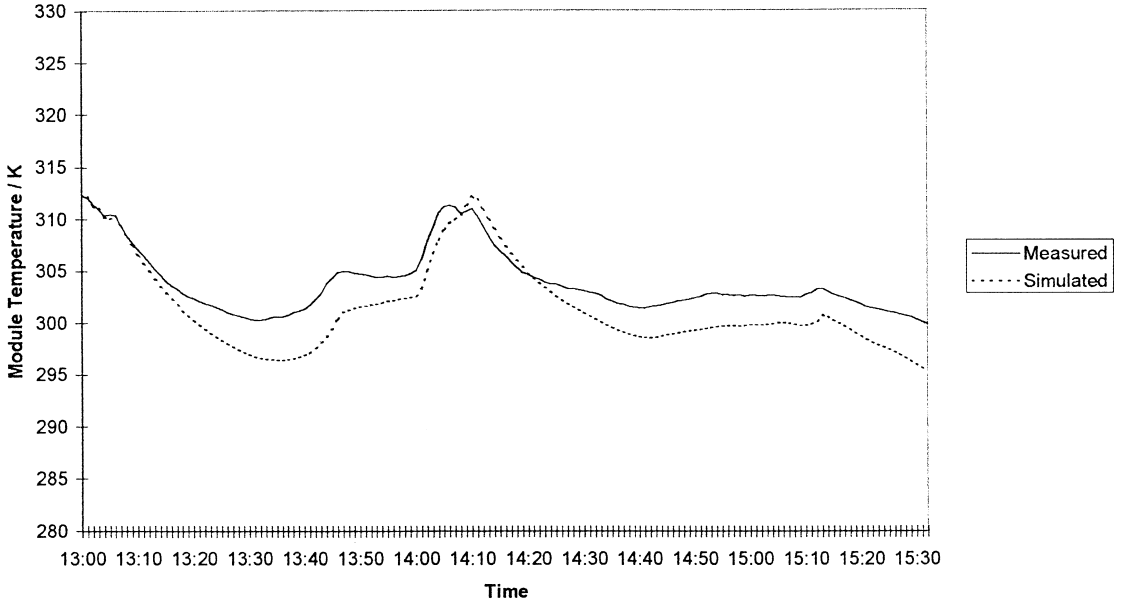

Fig. 6. Measured and simulated module temperature during period of cloudy sky conditions (data from 12/8/96).

are of similar magnitudes, having a magnitude of a quarter of the short wave radiation effect on the rate of temperature change. Under low irradiance (i.e. overcast and some cloudy periods), the short wave proportion drops by about one third, but remains the largest heat transfer path. The long wave contribution drops to the lowest contribution, due to the increase in effective sky temperature (Eq. (11)), this slows the module energy loss through emission under these conditions. The convection contribution also decreases during long periods of low irradiance, as the module temperature comes close to ambient temperature. The rate of change of thermal energy due to electricity production is also low, due to the decreased electrical output during periods of low irradiance.

It is worth noting that, during cloudy periods, the convection and long wave radiation contributions, being temperature dependent, change exponentially with time following rapid irradiance increases and decreases, whereas the electrical and short wave contributions, being irradiance dependent, track the variations in irradiance.

It is also observed that towards dusk on clear days the accuracy of the model decreases, with a tendency to underestimate module temperature. It is likely that during the evening period, the conditions of long wave radiation from the sky have changed from those described in Eq. (6). It is possible that ε_{sky} will increase as the sky darkens, thus decreasing the net output of long wave radiation from solar module to sky, which would increase module temperature above that estimated using the original model.

4.9. Estimation of initial values

Calculation of a series of module temperature values using the dynamic model requires an initial value of module temperature. So far, all calculations have used the measured value of temperature as the initial estimation. This does not realistically represent a situation of modelling blind, where actual temperature values are not available. In such cases, an estimation of module temperature may be made by using a steady state model. To avoid the 'worst case' scenario, when the initial estimation is made during an isolated peak or trough of irradiance which is not representative of the prevailing conditions, resulting in a severe over or underestimation of initial temperature, it is recommended that a preconditioning period of simulation for 30 time steps should be carried out. This will ensure that the contribution of a poor initial estimate to the uncertainty in the calculated value will be negligible.

5. TEMPERATURE MODELLING CONCLUSIONS

A model of module temperature based on environmental conditions is proposed, and has been adapted from previous authors' work. This model was a non-steady state equation of module temperature considering the various energy exchanges at the module. Each contribution is modelled according to theoretical considerations. The resulting model is a differential equation of the variation of module temperature with time according to climate conditions (Eq. (11)). A suitable method of numerically solving the equation was selected. The module temperature was solved for real data sets under a variety of conditions, and the time dependent behaviour of module temperature from the model was compared with that observed. The estimated and measured temperatures were correlated for a large number of data sets and the standard error of making an estimation obtained.

The response of the module temperature is dynamic with changes in irradiance, and to accurately model module temperature, particularly during periods of fluctuating irradiance, a dynamic model of module temperature is required. Steady state conditions have been observed to be atypical of module operating conditions over short time periods, and, in any case, a dynamic model naturally reduces to a static model under such conditions, making it suitable for the range of conditions met by the array.

It was found to be necessary to fit a value of the forced convection coefficient for module convection that was within the range predicted by previous authors. For comparison of different conditions it was necessary to have some information on the wind speed of the period. Unfortunately, wind speeds are not routinely recorded as part of the Northumberland Array monitoring system. The magnitude of the convection is represented in the model by the forced convection coefficient, $h_{\text{c,forced}}$. With the use of local data, the values of 2 W/m^2 K (for average periods, wind speed 2–4 m/s) and 4 W/m^2 K (for above average periods, wind speed 4+ m/s) were used. These values are within the lower end of the range that is generally suggested for estimated forced convection for the exterior of buildings.

There is some inevitable inaccuracy in the predicted values; it was found that the model is

effective in clear weather to within 5 K of measured values 95% of the time. The model responds to transient changes in irradiance with the same trend as the measured data, increasing the error in the predicted value slightly, compared to clear day data. It is noted that the model is slightly more precise under conditions of overcast irradiance. For an improved module temperature model, detailed experimental data would be needed.

This module temperature model was based on the work of previous authors. In this work it has been shown that, for 1-min time intervals, a steady state approach is inappropriate. The standard error of an estimate of module temperature is comparable to the 'average error' of 2 K given by Fuentes' (1984) model. The model presented here gives, however, a slightly larger error of temperature estimate in the cloudy and clear models than the 'weighted temperature difference' of 0.5 to 1.5 K in the similar model of Knaup (1992) (the weighted temperature difference gives an error value around 0.1–0.2 K lower than the standard errors given in Table 3). The dynamic approach adopted in the present work differs from the original steady state model of Schott (1985) on which it is based in other respects. The present model is thus recommended as suitable for PV power simulations for modelling time series data over short intervals such as exist under conditions of temporary cloudiness.

NOMENCLATURE

α	absorptivity of cell surface
ε	emissivity
ε_{ground}	emissivity of surface of ground
ε_{module}	emissivity of the PV module
ε_{sky}	emissivity of the sky dome
σ	Stefan–Boltzmann constant (5.669×10^{8} W/m^2 K^4)
Φ	total incident irradiance on module surface (W/m^2)
ρ_m	density of material (kg/m^3)
A	area of surface (m^2)
C_{FF}	fill factor model constant (1.22 K m^2)
C_m	Specific heat capacity of material (J/kg K)
C_{module}	module heat capacity (J/K)
d_m	depth of material in module (m)
E	incident irradiance (W/m^2)
F_{xy}	view factor, fraction of energy leaving surface x that reaches surface y
h_c	convection coefficient (W/m^2 K)
k_1	constant $=K/I_0$ ($=10^6$ m^2/W)
L_x	long wave irradiance emitted per unit area for surface x (W/m^2)
P_{out}	DC electrical power generated by module (W)
q_{conv}	rate of net energy exchange at module by convection (W)
q_{lw}	net rate of long wave energy exchange at module surface (W)
q_{sw}	net rate short wave energy exchange at module surface (W)
step	time step interval (s)
T	temperature (K)
$T_{ambient}$	ambient temperature (K)
T_{ground}	ground temperature (K)
T_{module}	module temperature (K)
T_{sky}	effective sky temperature (K)

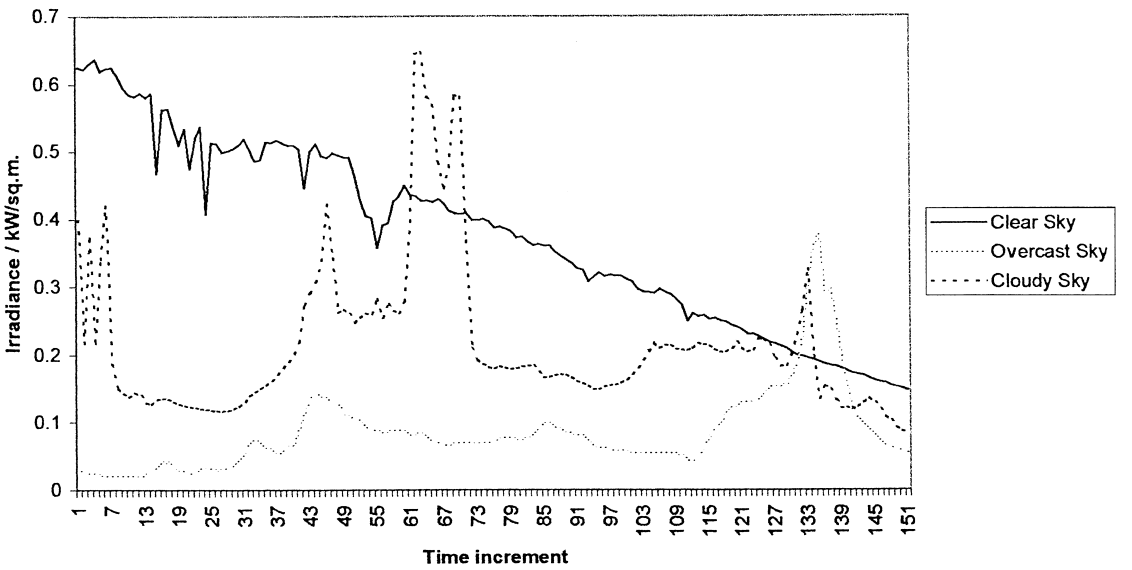

Fig. A1. Irradiance values for clear, overcast and cloudy sky examples.

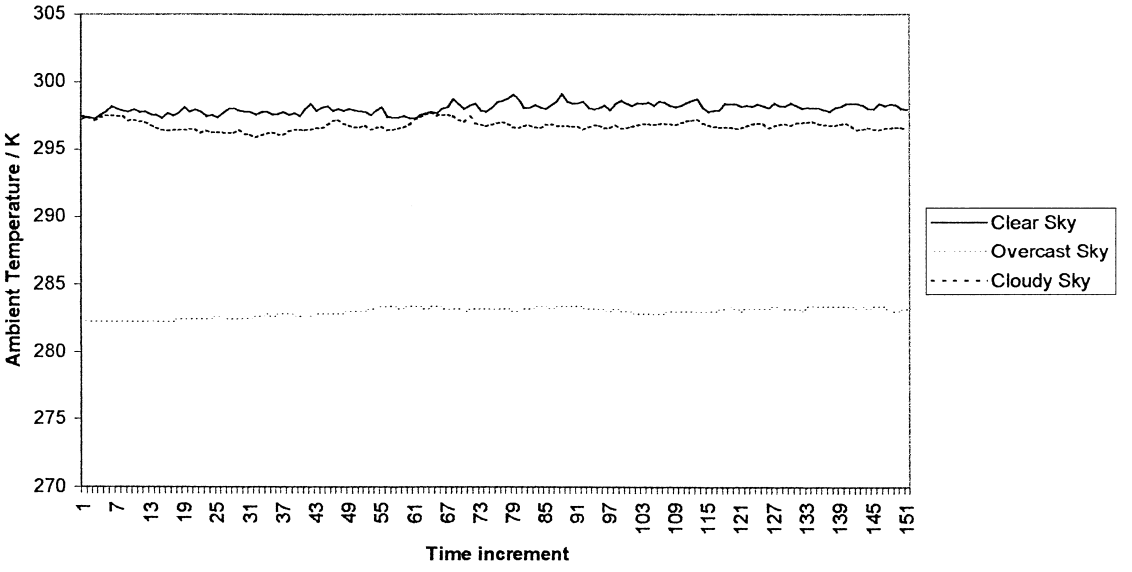

Fig. A2. Ambient temperature data for clear, overcast and cloudy sky examples.

Table A1. Hourly mean wind speeds for clear, overcast and cloudy examples (Met Office, 1995)

	(Hour commencing) Mean wind speed (m/s)			
Clear (15th August)	(13:00) 2.7	(14:00) 2.5	(15:00) 3.1	(16:00) 3.0
Overcast (1st November)	(09:00) 6.4	(10:00) 5.7	(11:00) 6.1	–
Cloudy (12th August)	(13:00) 2.0	(14:00) 2.5	(15:00) 2.9	–

Acknowledgements—All data for the model validation were provided by the Northumbria Photovoltaics Application Centre, whose help is appreciated.

APPENDIX

The appendix contains Figs. A1 and A2 and Table A1 giving the ambient temperature, irradiance and wind speed data for the examples used.

REFERENCES

Anis W. R., Mertens R. P. and Van Overstraeten R. (1983) Calculation of solar cell operating temperature in a flat plate PV array. In *5th E.C. PV Solar Energy Conference*, pp. 520–524.

ASHRAE (1989). *ASHRAE Handbook: Fundamentals.*

BP Solar (1999). *BP585 Photovoltaic module data sheet*, BP Solar, 30 Bridge St., Leatherhall, Surrey UK.

Fuentes M. K. (1984) Thermal model of residential photovoltaic arrays. In *17th IEEE PV Specialists Conference*, pp. 1341–1346.

Hill R. and Pearsall N. (1994) Architecturally integrated PV façade for commercial building in North East England. In *12th E.C. PV Solar Energy Conference.*

Holman J. P. (1992). *Heat Transfer*, McGraw-Hill.

James A.U. and Lord U.P. (1992). *MacMillans Chemical and Physical Data*, MacMillan Press.

Knaup W. (1992) Thermal description of photovoltaic modules. In *11th E.C. PV Solar Energy Conference*, pp. 1344–1347.

Liu B. Y. H. and Jordan R. C. (1963) The long term average performance of flat-plate solar energy collectors. *Solar Energy* **7**(2), 53–73.

Merrigan U.P. (1982). *Sunlight to Electricity*, MIT Press.

Met Office (1995). *Newcastle hourly wind speed data supplied by Newcastle Met Office.*

NPAC (1997) Private Communication with Newcastle Photovoltaics Application Centre.

Pratt A.W. (1981). *Heat Transmission in Buildings*, Wiley, London.

Schott T. (1985) Operational temperatures of PV modules. In *6th PV Solar Energy Conference*, pp. 392–396.

Wilshaw A. R., Bates J. R. and Pearsall N. M. (1996) Photovoltaic module operating temperature effects. In *Proceedings of Eurosun 96*, pp. 940–944.